Journal Name

ARTICLE

Influence of Different Liquid Environments on Atomic Force Microscopy Detection of Living bEnd.3 Cells

Received 00th January 20xx,
Accepted 00th January 20xx

DOI: 10.1039/x0xx00000x

www.rsc.org/

Jin Yan [a,b], Baishun Sun [a,b], Chenchen Xie [a,b], Yan Liu [a,b], Zhengxun Song [a,b], Hongmei Xu [a,b], and Zuobin Wang [a,b,c,*]

Atomic force microscope (AFM) is one of the most important tools in the field of biomedical science, which can be used to perform the high-resolution three-dimensional imaging of samples in a liquid environment and obtain their physical properties (such as surface potentials and mechanical properties). The influence of the liquid environment on the image quality of the sample and the detection results cannot be ignored. In this work, the QI mode AFM imaging and mechanical detections were performed on mouse brain microvascular endothelial (bEnd.3) cells in different liquid environments. The gray-level variance product (SMD2) function was used to evaluate the imaging quality of the cells in liquids with different physical properties, and the variations in cell mechanical properties were quantitatively analyzed. We introduced an AFM detection liquid containing less ions and organics, compared with the traditional culture medium, it is beneficial to improve the imaging quality, and have the similar mechanical detection results within three hours (3 h). It can greatly save the detection costs, and has positive significance in the AFM living cell detection.

1. Introduction

AFM is able to flexibly conduct the experiments in different situations (such as ambient air, vacuum and liquid environment). Liquid AFM has unprecedented temporal and spatial resolution (nanometer spatial resolution[1] and millisecond temporal resolution[2]) and its ability to acquire images in liquids has broadly expanded the scope of experimental design. These characteristics make liquid AFM have in situ advantages when detecting biological samples compared to other techniques (such as electron microscopy).[3-4] It is known that biological processes are carried out in a liquid environment. Using AFM to detect living cells under near-physiological conditions can characterize the surface morphology and the basic structure of cells, observe some dynamic physiological and chemical reactions. Therefore, real-time monitoring of the specific effects of drugs on living cells can be achieved, and it can provide intuitive evidences for studying the mechanism of drug action.[5-6]

AFM morphological imaging can visualize the fine structure of a single living cell,[7-10] achieve size measurement of nanoparticles,[11] and observe the influence of antibacterial agents on the microbial cell morphology[12] and the dynamic process at the molecular level[13]. Liquid AFM has been used in situ to study the effects of different liquid environments, such as adjusting pH or ion concentrations to investigate the nano-scale changes on the sample surface.[4,14] Electrostatic interaction significantly affects the AFM measurement of biomolecules[14]. The van der Waals force and electrostatic interaction between the tip and the sample can be balanced by adjusting the pH and the ionic strength of the buffer solution.[15-16] Imaging in liquid environments can reduce or eliminate capillary and van der Waals forces between the tip and the sample.[17-18] Samples observed in different environments may show different morphologies and structures. For example, bacteria imaged in the liquid have a smooth surface, but they show different structures in air.[19] Performing AFM experiments in a liquid environment is beneficial to improve the imaging resolution. Liquid imaging can reduce sample interference and minimize or prevent the damage due to the tip-surface shear forces. In the tapping mode, due to the reduction of the sample contact time, the vertical force is decreased, while the lateral force is almost ignored, which can reduce the sample damage and the image blur, improve the imaging quality.[20] When a researcher needs to obtain the imaging and mechanical properties of the sample via the AFM working in the classical modes (contact and tapping mode), two different experiments must be performed separately. However, switching from one mode to another, the correlation between the localization of mechanical properties and the image may be lost.[21-22] When an AFM in the QI mode is imaging biological samples, a whole force curve is measured at every pixel of the selected sample region simultaneously, which solves this problem well and also makes it common to be used for the detection of the characteristics of living cells.[23-

[a] International Research Centre for Nano Handling and Manufacturing of China, Changchun University of Science and Technology, Changchun 130022, China
[b] Ministry of Education Key Laboratory for Cross-Scale Micro and Nano Manufacturing, Changchun University of Science and Technology, Changchun 130022, China
[c] IRAC & JR3CN, University of Bedfordshire, Luton LU1 3JU, UK
†Corresponding author: Zuobin Wang, E-mail: wangz@cust.edu.cn

[24] By adjusting the physical parameters of the liquid medium, high-quality nano-processing based on AFM can be achieved.[25] Liquid AFM is a necessary method to image and manipulate the biological specimens, and has become an indispensable tool in biomedical research.[26] As the application of liquid media in AFM operations becomes more extensive, the influence of different liquids on AFM cell detection becomes unignorable. However, there are few related reports in this part. When using an AFM to detect cells, the cell culture medium mixed serum is usually used as the cell detection liquid. Commercial cell culture media contains a variety of inorganic salt ions, proteins, amino acids, glucose, hormones and other substances, which can meet the growth and metabolism needs of cells but are not conducive to AFM high-quality cell imaging and mechanical detection.

In this work, different liquids are selected as the environment for AFM detection to investigate the effects of different liquid physical environments on the imaging quality and the mechanical detection of bEnd.3 cells. We introduce a cell detection liquid, which can improve the quality of AFM cell imaging and provides similar mechanical detection results compared with the cell culture medium. This work provides the support for the study of liquid media and has significance for the study of the structure and function of biological cells.

2. Materials and methods

2.1 Physics principles

When a liquid AFM is in the scanning process, the drag force F_d exerted by the liquid on the probe can be expressed as: [27-28]

$$F_d = \frac{4\pi\eta L v}{\log\left(\frac{7.4}{Re}\right)} \quad (1)$$

η is the solution viscosity, L is the length of the cantilever, v is the velocity of the probe movement, and Re is the Reynolds number. When the probe cantilever is approaching to the cell surface, the squeezing force F_s applied on the probe is:[28-29]

$$F_s = \frac{3}{8}\eta v L\left(\frac{1}{S}\right)^3 \quad (2)$$

S is the normalized gap, which is the ratio of the cantilever-sample height to the cantilever width. When the probe is scanning laterally, shear force and friction force are also applied to the probe cantilever. Here the friction force is regarded as the sum of the shear stress and the loading force (F_n). Then, the comprehensive force F_C exerted on the cantilever can be expressed as:[30]

$$F_C = \eta L v_x\left[\frac{4\pi}{35\log\left(\frac{7.4}{Re}\right)} + \frac{3}{4} + \frac{1}{S}\right] + \left(\frac{\eta v_x A_t}{H - H_{tip}} + \alpha F_n\right) \quad (3)$$

The transition parameter α is a dimensionless coefficient in the range of 0-1.16. $(H - H_{tip})$ refers to the tip-sample distance. H_{tip} is the tip height. A_t is the tip contact area.

The tip-sample interactions can be regulated by changing the liquid composition. It can be approximated as:[31]

$$F_{el} = g_k\sigma_t\sigma_s e^{-kz} + g_{2k}(\sigma_t{}^2 + \sigma_s{}^2)e^{-2kz} \quad (4)$$

where the constant g_k is affected by the tip shape. The constant g_{2k} is influenced by the dielectric properties of the liquid. σ_t is the tip surface charges. σ_s is the sample surface charges. z is the tip-sample distance, k^{-1} is the Debye screening length:[32]

$$k^{-1} = \sqrt{\frac{\varepsilon_0\varepsilon_b k_B T}{2e^2 I}} \quad (5)$$

where ε_0 is the vacuum permittivity. ε_b is the liquid permittivity. k_B is the Boltzmann's constant. T presents the Kelvin temperature. I is the ionic strength of the liquid, which can be expressed as:[32]

$$I = \frac{1}{2}\sum_i z_i{}^2 c_i \quad (6)$$

Where z_i is the valence of ion i. c_i is the concentration of ion i.

2.2 Preparation of experimental liquids

In the experiment, the cell detective liquids contain three experimental groups and one control group. The experimental groups include phosphate-buffered saline (PBS), fetal bovine serum (FBS, Gibco), and potassium chloride with glucose injection (KCl+GS). RPMI-1640 with 10% FBS is the control group. RPMI-1640 and PBS are selected from HyClone. 10X concentrated PBS is used for preparing the PBS detective liquid. It is diluted 10 times with deionized water. The main ingredients are NaCl, $Na_2HPO_4.12H_2O$, KCl, and KH_2PO_4. Potassium chloride (10%) and glucose injection (5%) are purchased from the People's Hospital of Jilin Province. 5% GS and deionized water were made into 2.5% GS according to 1:1, and then 10% KCl and 2.5% GS were made into the cell detective liquid of experimental group according to 3:100 (KCl is at the concentration of 3.0 mg/ml).

2.3 Cell culture

The cover glass (18 mm×18 mm) was placed in a petri dish (38 mm diameter), and then the bEnd.3 cells were planted on it at the density of 1×10^4 cells/ml. RPMI-1640 with 10% FBS was used as the culture medium. Cells need to be cultured in a constant temperature incubator containing 5% CO_2 at 37 °C for 24 h.

2.4 Sample preparation

After 24 h incubation, the culture medium was discarded. The bEnd.3 cells were gently rinsed with PBS to remove the cell metabolites and unbound cells. 2 ml of the culture medium was added to each group of cells for AFM detection. After that, they were placed in air at 25 °C (consistent with the AFM detection environment) for 3 h and then used for optical imaging

2.5 MTT assay

After the cells were seeded in a 96-well plate (5.0×10^3 cells/well) and cultured for 24 h, the medium was replaced with the detective liquids (10 replicate wells for each group). The 96-well plate was placed in an air environment at 25 °C for 3 h, then 20 μl of MTT solution (5 mg/ml) was added to each well, and continued to culture in the incubator for 4 h. The solution was discarded, and 150 μl of dimethyl sulfoxide (DMSO) was added to each group well. Then a shaker was used

to shake the 96-well plate for 10 min to fully dissolve the blue-violet formazan crystals. Optical density (O.D) was obtained via a microplate reader at the wavelength of 498 nm.

3. Results and discussion

3.1 The influence of different liquids on AFM imaging quality

In this work, an AFM (JPK NanoWizard 3 BioScience) was used in the QI mode in liquid for the cell morphological imaging and the mechanical detection. The probe with a quadrangular pyramidal tip was purchased from Burker AXS (DNP-10, with the spring constant of 0.06 N/m, tip radius of 20 nm, and height of 5 μm). The thermal noise method was used to calibrate the spring constant of cantilever before the AFM detection. After the calibration, the cantilever spring constant was 0.058 N/m, the setpoint was 2 nN and the frequency of scanning was 0.8 Hz. AFM was running at the room temperature (25°C). JPK data processing (JPK Instrument, Berlin, Germany) software was used for the image and the force data processing.

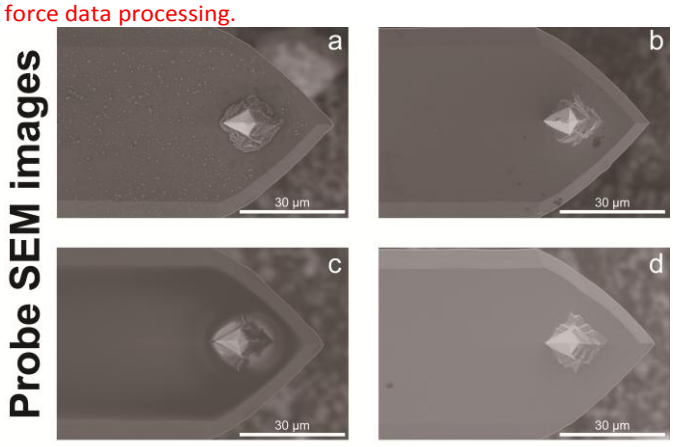

Fig. 1 SEM images of the AFM probe cantilever contamination after being immersed in different liquids for 3 h. SEM was working at the high vacuum mode (5000× magnification, spot: 3.0, HV: 3.00 kv, chamber pressure: 6.72 e-4 Pa).

In the experiment, the scanning electron microscope (SEM; Quanta 250, FEI) was used to image the probe to observe its contamination. **Fig. 1** shows the SEM images of the AFM probe (Budget Sensor, ContAl-G) after immersing in different liquids for 3 h. The probes have different degrees of adsorption. The most liquid component adsorption appears on the probe cantilever in PBS (**Fig. 1a**). In RPMI-1640+10% FBS, there are a small amount of stains on the cantilever (**Fig. 1b**). The film formed by serum components such as organic molecules can be clearly observed on the probe cantilever in FBS (**Fig. 1c**). But in KCl+GS, the probe cantilever keeps basically clean (**Fig. 1d**). The SEM images indicate that the KCl+GS has the least contamination to the probe.

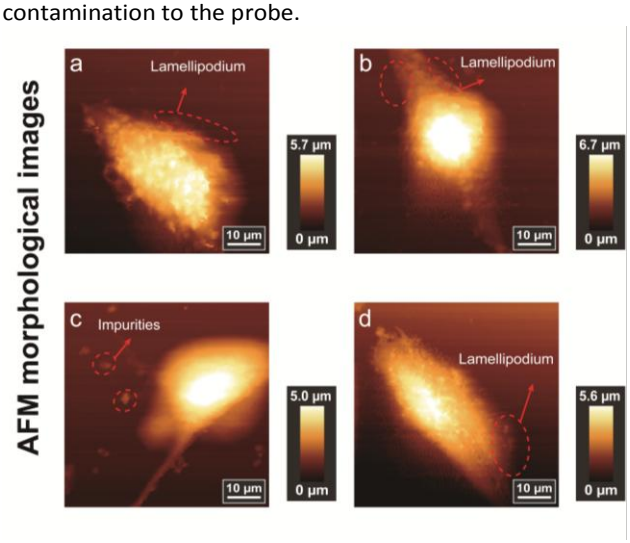

Fig. 2 AFM morphological images of bEnd.3 cells in PBS (a), RPMI-1640+10% FBS (b), FBS (c), and KCl+GS (d) in the QI mode. The scanning range is 60 μm× 60 μm.

Fig. 2 shows the AFM morphological images of the cells in the experimental groups and the control group with the same scanning parameters. The four groups of cells all present a long and narrow shape. The cell lamellipodium in KCl+GS (**Fig. 2d**) stretches well on the substrate, which is similar to the one of the control cells (**Fig. 2b**), The edge of the cell in PBS is irregular, and the lamellipodium appears to be contracted. The imaging of the cell in FBS is blurred, and visible impurities can be seen in the liquid. Various serum products (FBS, horse serum etc.) contain cholesterol, proteins, inorganic minerals and other substances, which easily lead to the formation of precipitates. These precipitates will have a negative impact on the AFM scanning and imaging. In order to quantify the imaging quality in different liquid environments, a quality assessment on the images was performed.

The resolution of AFM scanning image is an important index parameter to measure the quality of AFM image. SMD2 is a commonly used fast and high-sensitivity image sharpness evaluation function. The image SMD2 value is positively correlated with the image quality. It is defined as follows:[33]

$$D(f) = \sum_y \sum_x |f(x,y) - f(x+1,y)| \times |f(x,y) - f(x,y+1)| \quad (7)$$

where f(x,y) is the pixel value at the point (x,y) in the image.

The SMD2 function was used to evaluate the AFM images quality, as shown in **Fig. 3**. The SMD2 values of the AFM morphological images of the cells corresponding to **Fig. 2** are 501112 (PBS), 311154 (RPMI-1640+10% FBS), 280327 (FBS), and 610179 (KCl+GS) in sequence. The image quality of the cell in KCl+GS is the best of them. We have made statistics on the AFM imaging quality of each group of cells, and the results are as follows: SMD2 for the cell imaging in PBS is 527042.4±39335, in RPMI-1640+10% FBS is 377196.2±39177, in FBS is 296589.6±39829, and in KCl+GS is 548855.8±50123. The trend of SDM2 is the same as before, and the image quality of KCl+GS and PBS are significantly better than the rest two

groups which contain FBS. When the liquid media contain the serum, the force change between the tip and the sample caused by the kinematic viscosity of the fluid will affect the quality of AFM imaging. Serum will significantly increase the viscosity and concentration of the liquid,[30] which is consistent with the imaging quality evaluation results.

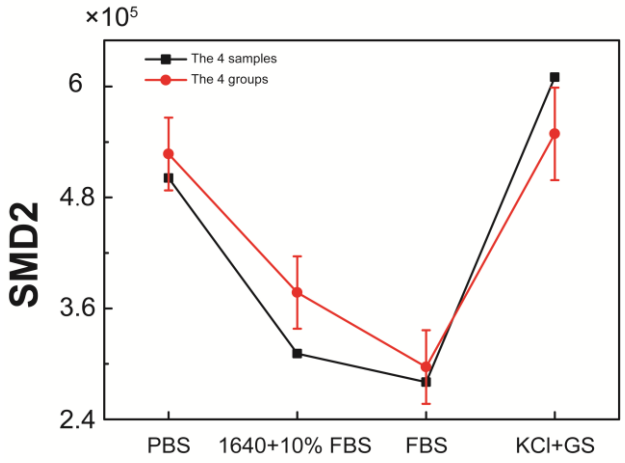

Fig. 3 AFM imaging quality evaluation curves of bEnd.3 cells in different liquids.

AFM test liquid should not only make the imaging quality as high as possible, but also maintain physical characteristics and viability of the cells during the detection process. We used the optical mode of Nikon microscope (Nikon ECLIPSE Ti) to obtain the optical images of cells. **Fig. 4** shows the optical images of the 4 group cells after exposing to air for 3 h. Most of the cells in the control group adhere well, and the cell has a long and narrow shape (**Fig. 4b**). Significant shrinkage of the cells can be observed in PBS (**Fig. 4a**), and the middle part of the cells changes into round. Some unbound cells are visible in the liquid. In FBS and KCl+GS, the cell morphology slightly shrinks, and a few unbound cells can be seen (**Figs. 4c-d**). Under the experimental conditions of this work, FBS and KCl+GS are better than PBS in maintaining cell morphology and activity. Serum contains growth factors to promote cell growth, and glucose is the major carbon and energy source for cell growth.[34-35] Potassium ion is the most abundant cation in the cell. There is a sodium-potassium pump on the cell membrane, which pumps sodium ions out of the cell and pumps potassium ions into the cell.[36] The results show that the appropriate concentration of potassium ions in the liquid can maintain cell viability and keep the volume of the cell in a short period of time (according to the experimental results, the time is less than 3 h, and the concentration of KCl is 3 mg/ml).

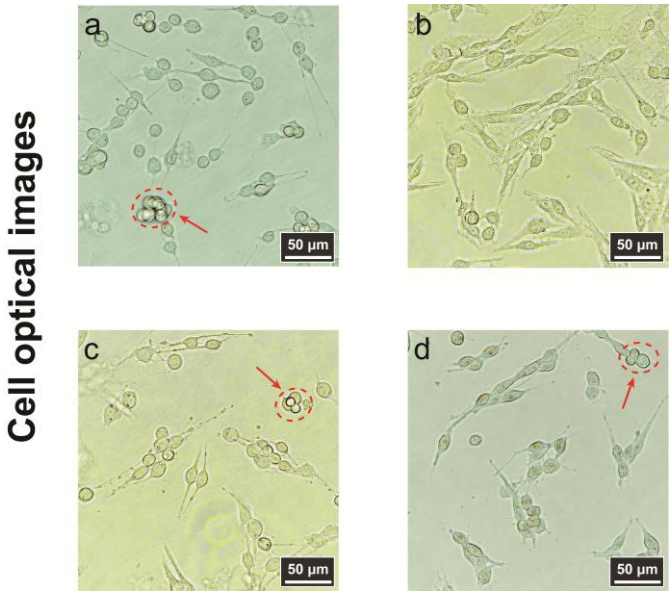

Fig. 4 The optical images at 40× magnification of bEnd.3 cells in PBS (a), RPMI-1640+10% FBS (b), FBS (c) and KCl+GS (d) after 3 h exposure to air.

Early studies have shown that the cell shrinkage and the average roughness is closely related to the cell viability.[37-38] During the process of drug-induced apoptosis, the average roughness of the cell membrane surface will also increase.[39-41] We selected 10 μm×10 μm from each cell surface for the RMS roughness measurement. The statistics about the influence of different liquids on the average roughness of the cell surface are shown in **Fig. 5a**. The cells in PBS (675.93±119.36 nm) is the largest of all. The control group is the smallest at 463.92±51.96 nm. The average surface roughness of the cells in FBS and KCl+GS are relatively close and both slightly larger than the one of the control group (564.70±56.05 nm for FBS and 580.12±86.23 nm for KCl+GS). As shown in the optical images (**Fig. 4**), the cell viability in PBS is weak, while the rest experimental groups are more similar with the control group. In order to verify this point, MTT assay was performed as shown in **Fig. 5b**. Optical density (O.D) reflects the cell activity. The O.D value of the control group is 0.62±0.07. It is the largest one in all the groups. The O.D value of cells in PBS is the smallest, which is 0.35±0.03. The one for FBS is 0.48±0.05 and 0.51±0.07 for KCl+GS. The results further illustrate that PBS is not conducive to maintain the cell viability, which is consistent with the previous work. FBS and KCl+GS can maintain good cell viability as the RPMI-1640 with 10% FBS.

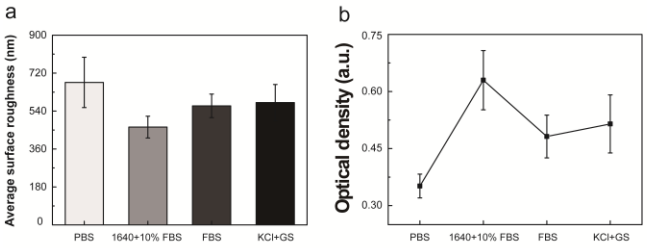

Fig. 5 The average surface roughness of bEnd.3 cells in different liquids (a). MTT assay of the cells in different liquids after exposing in air for 3 h (b). The results were expressed as the mean and standard deviation (±).

3.2 The influence of different liquids on cell AFM mechanics detection

The slope of the force-displacement curve depends on the cell stiffness. The greater the cell stiffness is, the steeper the curve is. **Fig. 6a** shows the results of the cell nano-indentation tests. The P points in the figure represent the probe tip successfully piercing into the cell membrane. The curve of the cell in PBS is the steepest, and P0 is the highest. The cell in FBS is the second one. The curve of the cell in KCl+GS is relatively flat and the slope is similar with that of the cell in RPMI-1640+10% FBS. The positions of P3 and P1 are similar. The cell average penetration force and depth were detected as shown in **Fig. 6b**. The cell average penetration force and depth in PBS (2.08±0.30 nN and 1.46±0.28 μm) are the largest of all. Those of the cells in the control group are 0.91±0.20 nN and 0.75±0.13. 1.20±0.19 nN and 0.79±0.18 μm are for the cells in FBS. 1.26±0.16 nN and 0.81±0.17 μm are for the cells in KCl+GS. From the statistical analysis of the data, the results of the cell nano-indentation tests in KCl+GS are closer to those of the control group cells. It shows that the cell stiffness in this liquid is similar with the one in RPMI-1640+10% FBS.

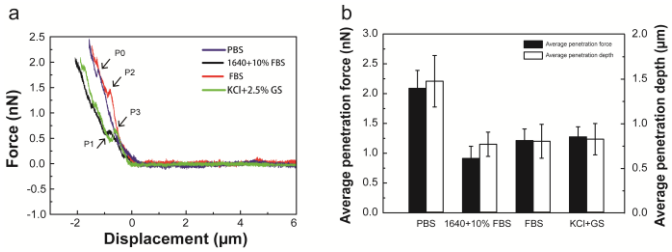

Fig. 6 The force-displacement curves of the cells in different liquids (a) and the statistical analysis of the average penetration force and depth of them (b). The results are given as the mean and standard deviation (±).

Elasticity measurement is very important for investigating the biophysical properties of cells.[42-44] AFM elastic modulus images of the cells in each group are shown in Figs. 7a-d. In order to investigate the influence of different liquids on the cell elastic modulus, we selected an area of 10 μm×10 μm on the cell surface, where the cell nucleus located, to detect the cell elastic modulus. We chose the Hertz model to perform the elastic modulus data analysis for each group of cells. The statistical distributions of 128×128 force data of the cells in PBS, RPMI-1640+10% FBS, FBS and KCl+GS are shown in **Figs. 7e-h**, respectively. The distribution of the elastic modulus of each cell is summarized in Table 1. Compared with the control cell, the cell in FBS has not been significantly changed in the 0-1 KPa area, while the rest two groups are decreased. In the area of 1-2 KPa, the elastic modulus distribution of the cell in KCl+GS is similar with that of the control group cell, and they both reach more than 80%. The elastic modulus distribution of the cell in FBS in this area drops by nearly a half. While the cell in PBS drops the most, with only 6.72% remaining. In the areas of 2-3 KPa, 3-4 KPa and >4 KPa, the elastic modulus distributions of the cells in KCl+GS change little, while the rest two experimental group cells increase obviously. It indicates that the cells in KCl+GS can better maintain the elastic modulus as the cells in RPMI-1640+10% FBS.

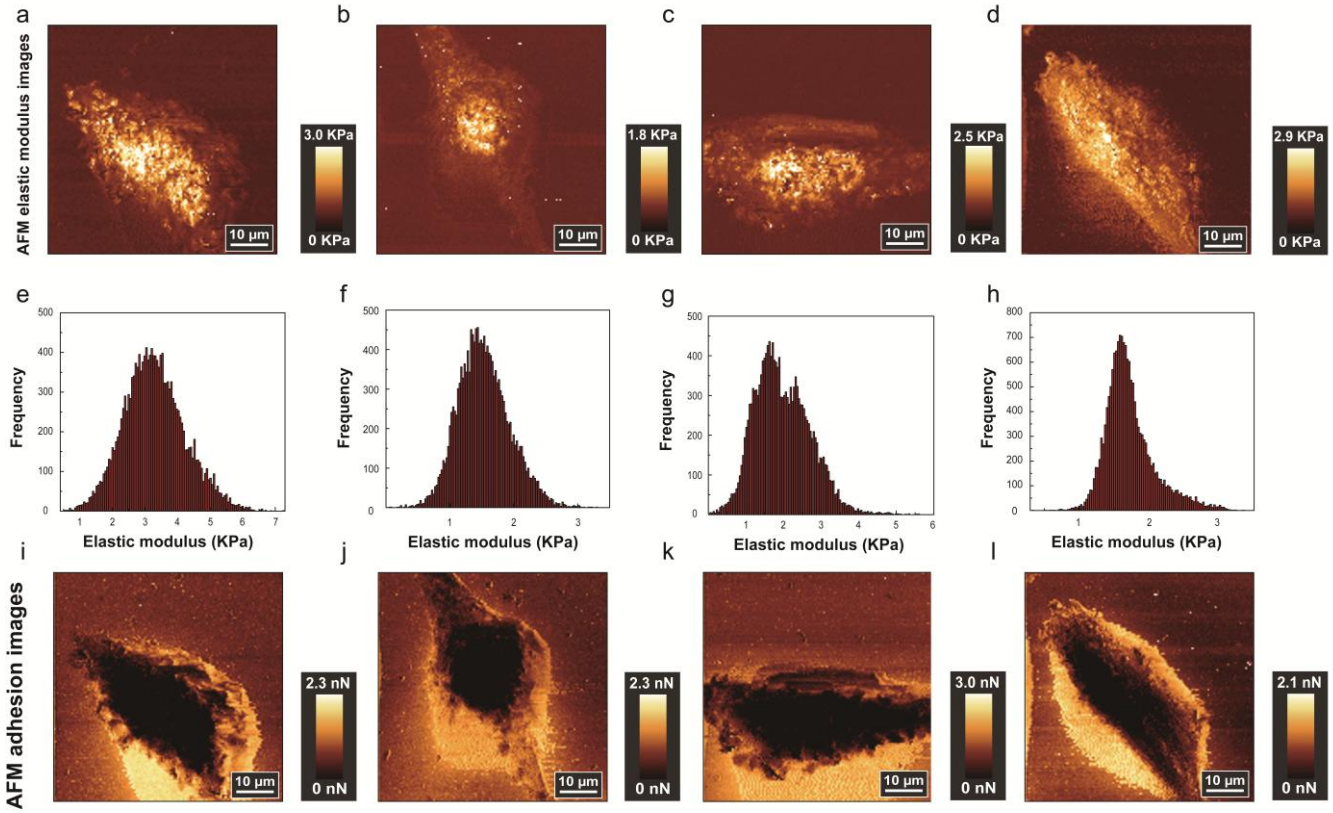

Fig. 7 AFM elastic modulus (a-d) and adhesion images (i-l) of bEnd.3 cells in PBS, RPMI-1640+10% FBS, FBS and KCl+GS in the QI mode, and the distributions of elastic modulus (e-h). The scanning range is 60 μm× 60 μm.

Table 1 Elastic modulus distributions of the cells in different liquids.

Group	0-1 KPa (%)	1-2 KPa (%)	2-3 KPa (%)	3-4 KPa (%)	>4 KPa (%)
PBS	0.32	6.72	33.07	38. 64	21.24
RPMI-1640+10% FBS	7.06	80.49	12.38	0.07	0
FBS	6.70	48.57	35.83	8.16	0.75
KCl+GS	0.46	82.02	17.08	0.45	0

The average cell elastic moduli in each group are shown in **Fig. 8a**. The cells in PBS have the largest average elastic modulus at 3.21±0.43 KPa, which is significantly increased compared with the control cells (1.61±0.21 KPa). The average elastic moduli of the cells in FBS and KCl+GS are similar, which are 2.09±0.29 KPa and 1.87±0.21 KPa. The average elastic modulus of the cells in KCl+GS is the closest to that of the control group cells.

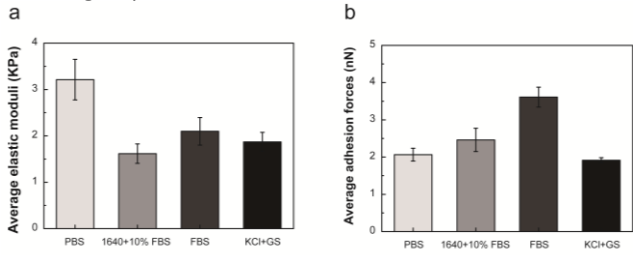

Fig. 8 Average elastic moduli of the cells in each group (a), and the average cell surface adhesion forces (b).

AFM adhesion images of the cells in each group are shown in **Figs. 7i-l**. In the experiment, we selected an area of 8 μm×8 μm on the cell surface to detect the cell surface adhesion force. **Fig. 8b** shows the average cell surface adhesion force in each group. The average cell surface adhesion force of the cells in FBS is 3.61±0.26 nN, which is significantly larger than that of the control cells (2.46±0.31 nN). Those in the rest two groups are less than that in the control group, and they are not significantly different from each other. (2.06±0.17 nN for PBS and 1.91±0.07 nN for KCl+GS). According to Eqs. 3-6, the forces of the probe cantilever in the liquid are closely related to the physical properties of the liquid under the condition of the same scanning parameters, which will directly affect the cell imaging quality and mechanical detection.

Conflicts of interest

There are no conflicts to declare.

Acknowledgements

This work was supported by National Key R&D Program of China (No.2017YFE0112100), EU H2020 Program (MNR4SCELL No.734174), Jilin Provincial Science and Technology Program (Nos.20180414002GH, 20180414081GH, 20180520203JH, 20190702002GH, and 20200901011SF), and "111" Project of China (D17017).

Conclusions

In this work, we performed AFM imaging and mechanical property detections on bEnd.3 cells in different liquids. By evaluating the imaging quality and analyzing the mechanical properties, the results show that the factors which cause the differences in AFM imaging quality are the liquid physical properties, which include viscosity, concentration, ion species and other parameters. The mechanical properties are closely related to the cell viability. The detection liquid of KCl+GS can maintain the cell viability within 3 h. The amounts of the ions and organic matter contained in the liquid are less than those of the traditional culture media, which can improve the quality of AFM imaging. The obtained cell mechanical properties are also similar with those of the cells in the traditional media. The investigation on AFM detection liquids helps to reduce the cost of the detection and provides supports for the high-quality imaging of biological samples under liquid phase conditions.

Notes and references

1. F. Oesterhelt, D. Oesterhelt, M. Pfeiffer, A. Engel, H. E. Gaub and D. J. Müller, *Science*, 2000, **288**, 143-146.
2. T. Ando, T. Uchihashi and S. Scheuring, *Chem. Rev.*, 2014, **114**, 3120-3188.
3. M. Li, N. Xie, Y. Wang and L. Liu, *Nano Res.*, 2019, **12**, 703-718.
4. V. D. Lyles, W. K. Serem, J. J. Yu and J. C. *Surface Science Techniques*, Springer Series in Surface Sciences, Springer, Berlin, Heidelberg. 2013, **51**, https://doi.org/10.1007/978-3-642-34243-1_20
5. M. Li, L. Liu, N. Xi and Y. Wang, *BioNanoSci.*, 2016, **6**, 22-32, https://doi.org/10.1186/s12951-018-0428-0
6. X. Deng, F. Xiong, X. Li, B. Xiang, Z. Li, X. Wu, C. Guo, X. Li, Y. Li, G. Li and W. Xiong, *J. Nanobiotechnol.*, 2018,**16**, https://doi.org/10.1186/s12951-018-0428-0
7. H. Schillers, I. Medalsy, S. Hu, A. L. Slade and J. E. Shaw, *J. Mol. Recognit.*, 2016, **29**, 95-101.
8. E. Hecht, K. Thompson, M. Frick, O. H. Wittekindt, P. Dietl, B. Mizaikoff and C. Kranz, *Anal. Chem.*, 2012, **84**, 5716-5722.
9. R. D.Turner, S.Mesnage, J. K. Hobbs and S. J. Foster, *Nat. Commun.*, 2018, **9**, 1263.
10. M. Li, L. Liu, N. Xi, Y. Wang, X. Xiao and W. Zhang, *IEEE Trans. Nanobiosci.*, 2015, **14**, 84-94.
11. T. H. Yuki, G. Yukihiro and S. K. Kumiko, *Anal. Bioanal. Chem.*, 2018, **410**, 1525-1531.
12. F. D. Cécile, E. D. Raphaël and D. Etienne, *Semin. Cell Dev. Biol.*, 2018, **73**, 165-176.
13. E. A. Sosnov and A. S. Kochetkova, *J. Synch. Investig.*, 2018, **12**, 1310-1322.
14. D. J. Müller and A. Engel, *Biophys. J.*, 1997, **73**, 1633-1644.
15. D. J. Müller, D. Fotiadis, S. Scheuring, S. A. Müller and A. Engel, *Biophys. J.*, 1999, **76**, 1101-1111.
16. T. J. Senden and C. J. Drummond, *Colloids & Surfaces A Physicochemical & Engineering Aspects*, 1995, **94**, 29-51.
17. Constant A. J. Putman, Kees O. Van der Werf, Bart G. De Grooth, Niek F. Van Hulst, and Jan Greve, *Appl. Phys. Lett.*, 1994, **64**, 2454, https://doi.org/10.1063/1.111597
18. M. Gauthier, S. Régnier, P. Rougeot and N. Chaillet, Patrick, *J. Micromechatronics*, 2006, **3**, 389-413.
19. M. J. Doktycz, C. J. Sullivan, P. R. Hoyt, D. A. Pelletier, S. Wu and D. P. Allison, *Ultramicroscopy*, 2003, **97**, 209-216.
20. M. H. Korayem and H. J. Sharahi, *Int. J. Adv. Manuf. Technol.*, 2011, **57**, 477-489.
21. G. Smolyakova, C. Formosa-Dagueb, C. Severaca, R.E. Duvalc and E. Daguea, *Micron*, 2016, **85**, 8-14.
22. L. Chopinet, C. Formosa, M.P.Rols, R.E. Duval and E. Dague, *Micron*, 2013, **48**, 26-33.
23. K. Casdorff, T.Keplinger and I. Burgert, *Plant Methods*, 2017, **13**, 60.
24. E. Rozhina, A. Panchal, F. Akhatova, Y. Lvov and R. Fakhrullin, *Appl. Clay Sci.*, 2020, **185**, 105371.
25. N. Amro, S. Xu and G. Liu, *Langmuir*, 2000, **16**, 3006-3009.
26. M. H. Korayem and A. Nahavandi, *Appl. Phys. A*, 2017, **123**, 265, https://doi.org/10.1007/s00339-017-0812-x
27. Y. Kim and J. Yi, *J. Phys. Chem. B*, 2006, **110**, 20526-20532.
28. R. E. Jones and D. P. Hart, *Tribol Int.*, 2005, **38**, 355-361.
29. H. J. Butt, B. Cappella and M. Kappl, *Surf. Sci. Rep.*, 2005, **59**, 1-152.
30. Y. Liu, Z. Wang, Y. Qu, Y. Lei, Y. Peng, P. Zhang, J. Liu, W. Jiang and Y. Bai, *3M-NANO*, **2012**, 14-17, DOI: 10.1109/3M-NANO.2012.6473002
31. H. J. Butt, *Biophys. J.*, 1991, **60**, 777-785.
32. B. W. Hoogenboom, *Bhushan B. (eds) Encyclopedia of Nanotechnology. Springer, Dordrecht*,2016, https://doi.org/10.1007/978-94-017-9780-1_108
33. F. Wang, P. Cao, Y. Zhang and H. Hu, *IEEE T. Instrum. Meas.*, 2020, **70**, 1-11.
34. E. H. Mathews, B. A. Stander, A. M. Joubert and L. Liebenberg, *Nutrition*, 2014, **30**, 218-227.
35. H. Y. Lee, Y. Itahana, S. Schuechner, M. Fukuda, H. S. Je, E. Ogris, D. M. Virshup and K. Itahana, *Sci. Signal.*, 2018, **11**, 7893.
36. A. Bueno-Orovio, C. Sánchez, E. Pueyo and B. Rodriguez, *Pflugers Arch-Eur J. Physiol.*, 2014, **466**, 183-193.
37. J. F. Kerr, A. H. Wyllie and A. R. Currie, *Br J. Cancer*, 1972, **26**, 239-257.
38. C. D. Bortner and J. A. Cidlowski, *Biochem. Pharmacol.*, 1998, **56**, 1549-1559.
39. K. Buyukhatipoglu and A. M. Clyne, *J. Biomed. Mater. Res. A*, 2011, **96**, 186-195.
40. D. C. Wang, K. Y. Chen, C. H. Tsai, G. Y. Chen and C. H. Chen, *J. Biomech.*, 2011, **44**, 2790-2794.
41. Y. Wang, C. Xu, N. Jiang, L. Zheng, J. Zeng, C. Qiu, H. Yang and S. Xie, *Scanning*, 2016, 38, 558-563.
42. Y. Liu, Z. Wang, and X. Wang, *J. Mech. Behav. Biomed. Mater.*, 2015, **45**, 65-74.
43. P. Carl and H. Schillers, *Pflugers Arch-Eur. J. Physiol.*, 2008, **457**, 551.
44. M. H. Korayem, Y. H. Sooha and Z.Rastegar, *J. Braz. Soc. Mech. Sci. Eng.*, 2018, **40,** 297.